https://doi.org/10.70882/hazwz584
SCIENCE FORUM (JOURNAL OF PURE AND APPLIED SCIENCES) 26, (5 Special) (2026), 218 - 233

Science Forum (Journal of Pure and Applied Sciences)

Journal Homepage: https://atbuscienceforum.com.ng/index.php/jpas

Optical Dispersion, Band-Gap Engineering and Structural Disorder in Er_2O_3/Er_2O_3 Nanoparticle-Doped Zinc Borotellurite Glasses for Photonic Applications

Ibrahim Abdullahi Inuwa[1,2], Abdullahi Usman[1], Dahiru Garba Diso[1], Mohammed Shitu[1,2]

[1]*Department of Physics, Faculty of Science, Aliko Dangote University of Science and Technology Wudil Kano*

[2]*Department of Physics, Federal College of Education, Yola. Adamawa*

Abstract

Zinc borotellurite glasses with nominal composition $\{[(TeO_2)_{0.65}(B_2O_3)_{0.35}]_{0.65}(ZnO)_{0.35}\}_{1-x}(Er_2O_3$ or Er_2O_3 nanoparticles$)_x$ (x = 0.005–0.030) were synthesised by melt quenching to compare conventional and nanoparticle dopants in optical dispersion, band-gap characteristics, and structural disorder. X-ray diffraction confirmed the amorphous nature of both synthesized glass series. Transmission electron microscopy showed well-dispersed Er_2O_3 nanoparticles measuring approximately 10–20 nm, while energy-dispersive X-ray spectroscopy confirmed the constituent elements. Fourier-transform infrared spectra revealed concentration-dependent changes in TeO_4/TeO_3 and BO_3/BO_4 structural units, indicating modifications to local bonding. Er_2O_3 incorporation increased density and decreased molar volume; nanoparticle-doped glasses were denser than conventionally doped counterparts. Optical absorption spectra exhibited characteristic Er^{3+} 4f–4f transitions, including $^4I_{15/2} \rightarrow {}^4I_{13/2}$ near 1.53 µm. Refractive index increased with dopant concentration and was consistently higher for nanoparticle-doped glasses. Tauc analysis showed that the indirect optical band gap decreased from 2.954 to 2.568 eV in the conventional Er_2O_3 series and from 3.061 to 2.390 eV in the nanoparticle series. Correspondingly, Urbach energy increased from 0.315 to 0.675 eV and from 0.340 to 0.800 eV, respectively. Concurrent band-gap narrowing and Urbach-tail broadening indicate dopant-induced changes in local bonding and increased structural and electronic disorder, more pronounced with nanoparticle incorporation. These measurements collectively enabled comparison of dopant-dependent changes across the investigated compositions and provided complementary evidence linking the observed optical-edge evolution with concentration-dependent structural modifications in both glass series. These results demonstrate that Er_2O_3 nanoparticle doping can tailor refractive-index dispersion and the optical absorption edge in zinc borotellurite glasses, supporting their potential for near-infrared photonic and fibre-optic applications.

Keywords

Zinc Borotellurite Glass; Structural Disorder; Band-Gap Engineering; Photonic; Photoluminescence

EISSN: 3156-5190 (Online)
ISSN: 1119-4618 (Print)
JPAS
Faculty of Science, ATBU Bauchi

Corresponding Author: Ibrahim Abdullahi Inuwa, *Department of Physics, Faculty of Science, Aliko Dangote University of Science and Technology Wudil Kano* Email: *Ibrahiminwa2013@gmail.com*, © 2026 Faculty of Science, ATBU Bauchi. All rights reserved

1. Introduction

Tellurite-based glasses are attractive host materials for photonic applications because of their high refractive index, broad infrared transmission range, good rare-earth-ion solubility, relatively low phonon energy, and comparatively low processing temperatures (Lemière et al., 2022; Preethi et al., 2026). Among these materials, zinc borotellurite glasses offer a versatile network in which the incorporation of B_2O_3 and ZnO into TeO_2 can modify glass-forming ability, structural connectivity, chemical durability, and the local environment of optically active ions. B_2O_3 generally promotes network formation and suppresses crystallisation, whereas ZnO can participate in network modification and influence the coordination and bonding environment of the glass constituents (Ngaram et al., 2025; Preethi et al., 2026).

Er^{3+} is particularly important for near-infrared photonic applications because the $^4I_{13/2} \rightarrow {}^4I_{15/2}$ transition produces emission near 1.53 μm, within the low-loss telecommunications window. Consequently, Er^{3+}-doped glasses have been widely investigated as active media for fibre amplifiers, fibre lasers and other integrated photonic devices (Kraskowski et al., 2025; Ngaram et al., 2025). The 4f–4f transitions of Er^{3+} also generate characteristic absorption and emission bands extending across the visible and near-infrared regions. Their spectroscopic response is strongly influenced by the host-network structure, local asymmetry, bonding environment and concentration of the rare-earth ions. In oxide glasses, Er^{3+} incorporation can modify the oxygen-bonding environment and the relative populations of different network structural units, thereby affecting the polarizability, refractive index and electronic absorption edge of the host.

The use of rare-earth oxide nanoparticles as dopant sources provides an additional route for modifying the local structure and optical response of glass hosts. Compared with conventional bulk or microparticulate oxide incorporation, nanoscale Er_2O_3 may introduce distinct particle–matrix interfaces and local-field environments, which can influence dopant distribution, absorption strength and radiative or non-radiative processes (Preethi et al., 2026). The resulting effects are expected to depend strongly on nanoparticle concentration and the interaction between the dispersed phase and the glass network. Comparative investigation of conventional Er_2O_3 and Er_2O_3 nanoparticle incorporation is therefore important for distinguishing the effects associated with dopant concentration from those arising from the physical form of the dopant.

Beyond luminescence, the optical response of rare-earth-doped glasses can be evaluated through refractive-index dispersion, optical band gap and Urbach energy. Refractive-index dispersion is a fundamental parameter in photonic-device design because it influences light confinement, propagation and device dimensions. The refractive index and its wavelength dependence are governed by the composition, density, bonding characteristics and electronic polarizability of the glass network. Similarly, compositional modification can alter the optical band gap through changes in local bonding, electronic polarizability and the distribution of localized states. In rare earth doped oxide glasses, the addition of modifier species can lead to structural rearrangements and modify the non-bridging-oxygen environment, which could be the cause for the observed shifts in the absorption edge and the optical band gap (Ngaram et al., 2025; Preethi et al., 2026).

The amount of disorder connected with these structural modifications is measured by the Urbach energy, E_U, which is defined as the exponential absorption tail extending below the optical absorption edge. An increase in E_U typically suggests increased band-tail broadening due to structural and electronic disorder, such as variations in bond lengths, bond angles, and local bonding environments. Therefore, the simultaneous analysis of the refractive-index dispersion, the optical band gap and the Urbach energy gives a more complete description of the relationship between the composition, the structural disorder and the optical response than

the consideration of one parameter alone. The literature reports a large number of studies on Er^{3+}-doped tellurite and borotellurite glasses, but the combined effect of conventional Er_2O_3 and Er_2O_3 nanoparticle addition on the optical dispersion, band-gap evolution and Urbach disorder in zinc borotellurite glasses has been relatively less studied (Preethi et al., 2026; Ngaram et al., 2025). Previous studies have predominantly focused on luminescence characteristics, Judd–Ofelt parameters and emission cross-sections, whereas the relationship between refractive-index dispersion, optical band gap and absorption-edge disorder has received less systematic attention, particularly for nanoparticle-containing glass systems. Accordingly, this study systematically investigates zinc borotellurite glasses doped with Er_2O_3 and Er_2O_3 nanoparticles over a controlled concentration range, with emphasis on their optical dispersion and electronic-structure evolution.

The specific objectives are to: (i) determine the concentration- and dopant-form dependence of the refractive index and related dispersion parameters; (ii) evaluate the direct and indirect optical band gaps using Tauc analysis; (iii) quantify absorption-edge disorder through the Urbach energy; and (iv) establish correlations among dopant incorporation, refractive-index dispersion, band-gap modification and structural disorder. By combining these parameters within a common structure–property framework, the study provides insight into the optical response of Er_2O_3-modified zinc borotellurite glasses and identifies compositional regimes of interest for rare-earth-based photonic applications.

2. Experimental Details

2.1 Glass composition and sample preparation

Two series of zinc borotellurite glasses doped with conventional Er_2O_3 and Er_2O_3 nanoparticles were prepared using the conventional melt-quenching technique. High-purity analytical-grade starting materials TeO_2 (99.99% Alfa Aesar), B_2O_3 (99.98% MW 69.61), ZnO (99.99% Zink Oksider M.W 81.39, R&M Chemical), Er_2O_3 (99.9% Alfa Aesar), and Er_2O_3 nanoparticles were weighed according to the nominal composition. $\{[(TeO_2)_{0.65}\ (B_2O_3)_{0.35}]_{0.65}\ (ZnO)_{0.35}\}_{1-x}$ (Er_2O_3 NPs), where x = 0.005, 0.01, 0.015, 0.02, 0.025, and 0.03 molar fractions. The batches of about 15 g were ground thoroughly in an agate mortar to give homogeneity and placed in alumina crucibles. The mixtures were heated to 400 °C for 60 min to remove moisture and volatile impurities. Then it was melted at 950 °C and 1100 °C for 90 min with occasional stirring to obtain a homogeneous melt and to remove gas bubbles. The molten glass was rapidly quenched by pouring onto pre-heated stainless steel molds at 400 °C, followed by immediate annealing at 400 °C for 60 min to release internal stresses. Then the furnace was cooled slowly to room temperature. The obtained glass disks were polished to optical quality for further characterization (Hamza et al., 2022; Ngaram et al., 2025; Preethi et al., 2026).

2.2 Characterization techniques

2.2.1 Density and molar volume measurements

Density was measured at room temperature by the Archimedes principle using distilled water as the immersion liquid (accuracy ±0.001 g/cm³) and calculated using Eq. (1)

$$\rho = \frac{W_a}{W_a - W_b}\rho_{dw} \qquad 1$$

Where ρ_{dw} is the density of the immersed liquid, W_a is the weight of the glasses in the air, and W_b is the weight of the glasses in water. Three repeated measurements were made for each glass.

Molar volume (V_m) was calculated from the measured density and molecular weight of each composition using Eq. (2).

$$V_m = \frac{M_w}{\rho} \qquad 2$$

2.2.2 X-ray diffraction (XRD) analysis

XRD patterns were recorded on a powder diffractometer using Cu-Ka radiation (λ = 1.5406 Å) in the 2θ range of 10–80° to confirm the amorphous nature of the glasses.

2.2.3 Fourier-transform infrared (FTIR) spectroscopy

The structural units (TeO_4, TeO_3, BO_4, and BO_3) present in the glass network were identified by recording FTIR spectra in the range 400–4000 cm^{-1} by the KBr pellet technique.

2.2.4 Transmission electron microscopy (TEM) and energy-dispersive X-ray (EDX) spectroscopy

The morphology, size distribution and elemental distribution of the Er_2O_3 nanoparticles embedded in the glass matrix were investigated by transmission electron microscopy (TEM) at an accelerating voltage of 200 kV. The specimens for TEM were prepared by crushing a small amount of glass powder, dispersing it in ethanol under ultrasonication, depositing a drop of the suspension on a carbon-coated copper grid and then drying under ambient conditions. Average particle size and crystalline nature of the nanoparticles in the amorphous glass host were confirmed from high resolution TEM (HR-TEM) images. The energy dispersive X-ray (EDX) spectrum in combination with the TEM or scanning electron microscopy confirmed the presence and homogenous distribution of the constituent elements (Te, B, Zn, O and Er) and validated the successful incorporation of erbium nanoparticles into the glass network (Hamza et al., 2022; Preethi et al., 2026; Umar et al., 2020).

2.2.5 UV–Vis–NIR absorption spectroscopy

Optical absorption spectra were recorded at room temperature using a dual-beam UV–Vis–NIR spectrophotometer in the wavelength range 200–2000 nm. The absorption data were used to determine the optical band-gap energies (direct and indirect) via Tauc plots and to evaluate the Urbach energy as a measure of structural disorder.

$$\alpha = \frac{2.303A}{t} \quad (3)$$

where A is the measured absorbance and t is the sample thickness in cm.

The optical band gap energy (E_{opt}) was estimated using the Tauc relation for indirect transitions:

$$(\alpha h\nu)^{1/2} = B\left(h\nu - E_{opt}\right) \quad (4)$$

where $h\nu$ is the photon energy, and B is a constant. By plotting $(\alpha h\nu)^{1/2}$ versus $h\nu$ and extrapolating the linear region to intercept the energy axis, the optical band gap was obtained.

The Urbach energy (Eu), which indicates the width of the band tail and degree of structural disorder, was derived from the exponential region of the absorption edge using:

$$\alpha(h\nu) = \alpha_O \exp\left(\frac{h\nu}{E_u}\right) \quad (5)$$

2.2.6 Refractive index measurements

The refractive index of the polished glass samples was measured at room temperature using a high-precision spectroscopic ellipsometer (or, alternatively, by the Brewster-angle method) over the visible to near-infrared spectral range. For ellipsometric measurements, the amplitude ratio (Ψ) and phase difference (Δ) of the reflected light were recorded at multiple angles of incidence, and the refractive index dispersion was extracted by fitting the data to an appropriate optical model (e.g., Cauchy or Sellmeier dispersion relation).

When the Brewster-angle method was employed, the angle of incidence at which the p-polarized reflectance reached a minimum was determined, and the refractive index was calculated from the relation $n = tan\theta_B$, where θ_B is the Brewster angle. The obtained refractive-index values were further

used to calculate related optical parameters such as molar refraction, electronic polarizability, and metallization criterion (Azlan et al., 2017; Gowda et al., 2024; Ngaram et al., 2025).

3 Results and discussion

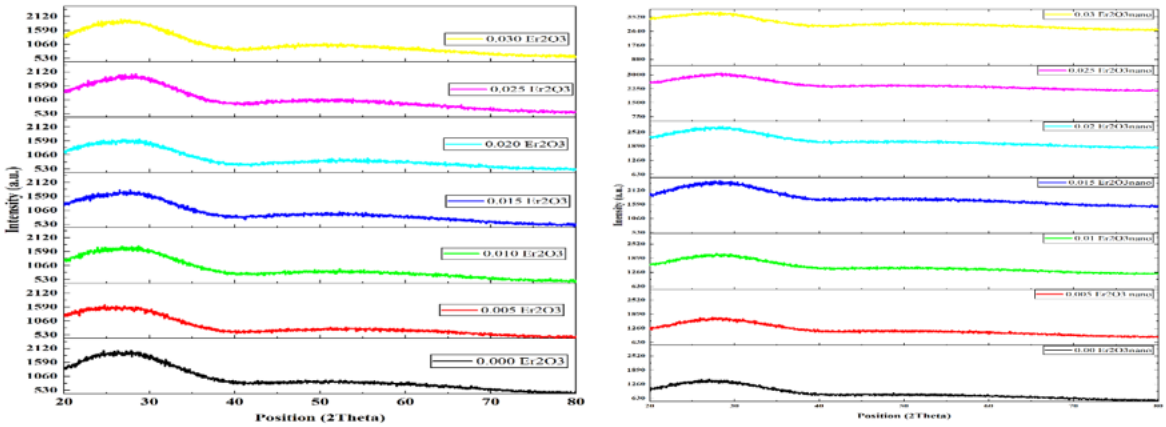
3.1 X-ray diffraction (XRD)

The X-ray diffraction (XRD) patterns presented in **Fig. 1** for the zinc boro-tellurite glass system with the nominal composition $\{[TeO_2]_{0.65}\ (B_2O_3)_{0.35}]_{0.65}\ (ZnO)_{0.35}\}_{1-x}\ (Er_2O_3\ /\ Er_2O_3\ NPs)_x$ exhibit characteristic features of amorphous materials. Both series (i) conventional Er_2O_3 doping and (ii) Er_2O_3 nanoparticle (NPs) doping display broad, diffuse scattering humps centred primarily in the low-angle region (approximately 20°– 40° 2θ), with no detectable sharp Bragg diffraction peaks across the measured range. This absence of discrete crystalline reflections confirms the long-range structural disorder inherent to the glassy state and verifies the successful formation of fully amorphous networks via the melt-quenching process.

The broad hump arises from short-range order associated with the primary network-forming units (primarily TeO_4/TeO_3 polyhedral and BO_3/BO_4 units modified by ZnO), consistent with the expected behaviour of multicomponent tellurite-based glasses. The intensity and position of the diffuse scattering remain largely invariant with increasing dopant concentration, indicating that neither bulk Er_2O_3 nor Er_2O_3 NPs induce detectable crystallization or phase separation under the applied synthesis conditions. These observations are in agreement with the vast literature on rare-earth doped zinc boro-tellurite and similar tellurite glass systems where XRD is routinely used to establish amorphicity before optical and spectroscopic characterization. Similar broad hump-shaped patterns without sharp peaks were reported for Er 3+ -doped and Er 2 O 3 -NP-doped zinc borotellurite glasses, suggesting that the incorporation of erbium (in conventional or nanoscale form) does not affect the vitreous network for the doping studied (Azlan et al., 2013; Azlan et al., 2016).

This interpretation is also supported by recent studies on analogous boro-tellurite and tellurite matrices. For example, X-ray diffraction (XRD) pattern of Er 3+ -activated telluro-borate and related systems have always shown only broad humps (generally at around 23°–35° 2θ) and not any crystalline reflections confirming the amorphous nature even with successive rare-earth addition (Ngaram et al., 2025). Structural analysis of the nanoparticle-doped variants confirms the existence of dispersed Er2O3 NPs in an amorphous matrix, and hence the XRD signature remains mostly characteristic of the disordered glass host rather than any crystalline nanoparticle contribution at low-to-moderate loadings (Azlan et al., 2024).

The amorphous signatures of the bulk Er_2O_3 and Er_2O_3 NPs series are analogous and suggest the same glass-forming ability and structural homogeneity. This is beneficial for photonic applications, since the absence of crystallinity reduces scattering losses and retains the high optical transparency and low phonon energy of the tellurite hosts. A comprehensive review of transition-metal-oxide nanoparticle and rare-earth-doped borate/tellurite glasses (Preethi et al., 2026) further highlights that amorphous XRD profiles are reliable indicators of network integrity for next generation optical technologies.



(i) XRD Patterns of Er_2O_3 (ii) XRD Patterns of Er_2O_3 NPs

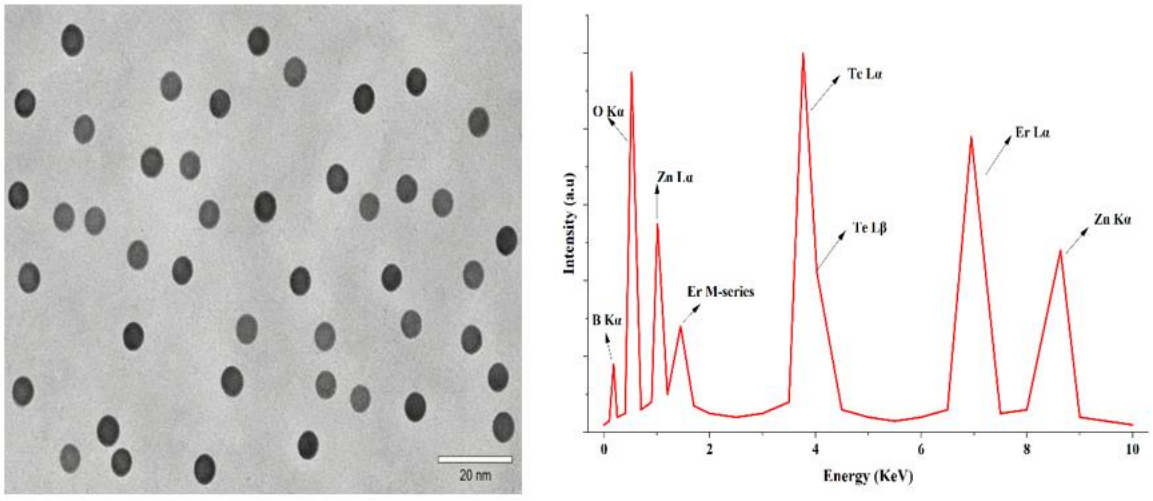
Fig. 1. XRD patterns of the new formulation of zinc boro-tellurite glass system for $\{[(TeO_2)_{0.65}(B_2O_3)_{0.35}]_{0.65}(ZnO)_{0.35}\}_{1-x}(Er_2O_3/Er_2O_3\ NPs)_x$ glass system.

3.2 Transmission electron microscopy (TEM) and energy-dispersive X-ray (EDX)

Fig. 2 (i) and (ii) present the transmission electron microscopy (TEM) image and the corresponding energy-dispersive X-ray (EDX) spectrum of Er_2O_3 nanoparticles (NPs) dispersed within the zinc boro-tellurite glass matrix. The TEM micrograph (panel i) reveals discrete, nearly spherical dark-contrast particles homogeneously distributed throughout the amorphous glass host. The particles are mostly of diameters in the range of about 10–20 nm (scale bar=20 nm) with little indication of significant agglomeration or clustering. This morphology is typical of well dispersed rare-earth oxide nanoparticles which retain their nanoscale dimensions when incorporated by melt-quenching. (ii) The corresponding EDX spectrum confirms the elemental composition of the glass system.

All the peaks corresponding to Te (La), Zn (Ka and La), O (Ka), B (Ka) and Er (La and M series) are clearly observed confirming the successful incorporation of all the nominal glass constituents and the presence of erbium from the Er2O3 NPs. No other elemental signals were detected, further confirming the purity of the synthesized materials. These findings are consistent with earlier investigations of Er2O3-NP doped zinc borotellurite and related tellurite glasses in which the presence and size distribution of nanoparticles (generally 15–30 nm) in the glass matrix were verified by TEM without inducing crystallization (Azlan et al., 2016; Azlan et al., 2013). In some cases, spherical or near-spherical nanoparticles of similar size are well distributed with limited Oswald ripening at higher loadings. The EDX/EDXRF confirms the presence of Te, Zn, B/O, Si (if present) and Er as reported in recent work on Er_2O_3 -NP-doped borotellurite silicate and tellurite systems (Hamza et al., 2020; Preethi et al., 2026).

The homogeneous distribution of Er_2O_3 NPs observed in this work is especially beneficial for photonic applications. The uniform nanoscale dispersion reduces light scattering, maintaining optical transparency and can increase local-field effects or energy-transfer processes involving the Er^{3+} ions that may, in turn, enhance the luminescence efficiency of fiber amplifiers, lasers and other Nano photonic devices. All the expected elements are confirmed simultaneously by EDX, confirming the stoichiometric integrity of the glass formulation.



(i) TEM image of Er_2O_3 nanoparticles (ii) EDX spectrum

Fig. 2. TEM image of Er_2O_3 nanoparticles embedded in the glass matrix and EDX spectrum confirming the presence of Te, Zn, B, O, and Er elements

3.3 Fourier transform infrared (FTIR)

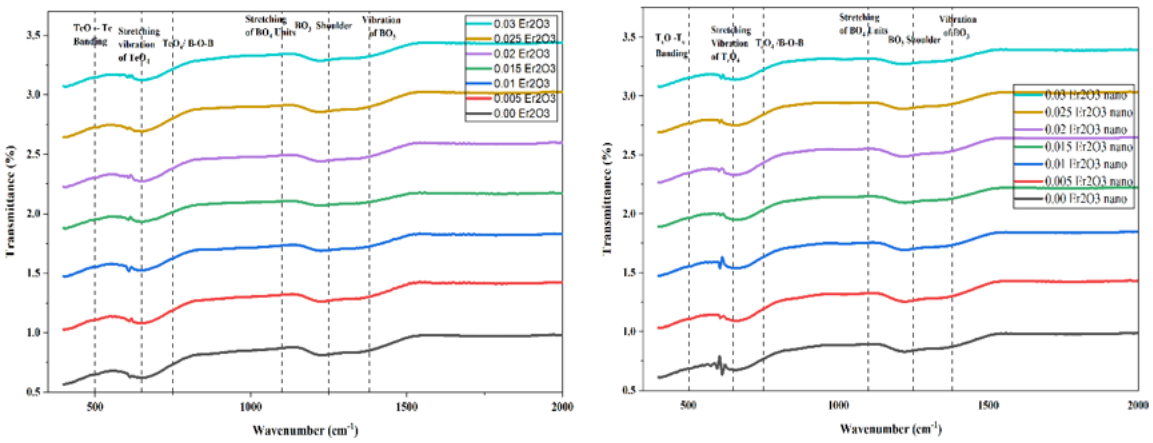
Fig. 3 presents the FTIR spectra of the zinc boro-tellurite glass system $\{[TeO_2]_{0.65}(B_2O_3)_{0.35}]_{0.65}(ZnO)_{0.35}\}_{1-x}(Er_2O_3 / Er_2O_3\ NPs)_x$, and Table 1 summarizes the principal absorption bands and their assignments for both the Er_2O_3-doped and Er_2O_3-nanoparticle-doped series, confirming that the incorporation of erbium in either form does not disrupt the fundamental glass network. The spectra show characteristic absorption bands at ~500 cm^{-1} (Te–O–Te bending), 650 cm^{-1} (stretching vibration of TeO_4 trigonal bipyramidal units), 750 cm^{-1} (overlap of TeO_4 stretching and B–O–B bending modes), 1100 cm^{-1} (Te–O stretching in TeO_3 units associated with non-bridging oxygen), 1250 cm^{-1} (BO_3 shoulder) and 1380 cm^{-1} (asymmetric stretching vibrations of BO_3 units).

These assignments are consistent with the established structural units of zinc borotellurite glasses. ZnO and rare-earth oxides act as network modifiers and promote the gradual conversion of TeO_4 to TeO_3 units and the formation of BO_3 groups, thereby increasing the concentration of non-bridging oxygen. Band positions and structural interpretations reported in recent studies on Er^{3+} and Er_2O_3- The NP-doped zinc borotellurite and related borotellurite systems are essentially similar, which confirms that the existence of both bulk and nanoscale erbium leads to a similar network modification without crystallization (Hamza et al., 2020; Rafie et al., 2020; Singh et al., 2024).

Minor intensification of the BO_3 band near 1380 cm^{-1} in the nanoparticle series suggests a slightly higher degree of local disorder or BO_4-to-BO_3 conversion arising from the greater surface reactivity of the nanoparticles, yet the overall spectral similarity demonstrates successful integration of both dopant forms into a homogeneous amorphous matrix. This structural configuration, rich in non-bridging oxygen, is advantageous for photonic applications because it lowers the effective phonon energy and enhances the local polarizability around Er^{3+} ions, thereby favoring efficient radiative transitions.

Table 1. FTIR results of Er_2O_3 and Er2O3NP-doped zinc borotellurite glass.

Glass system		Band Number (cm^{-1})	Band Assignments
(i)	Er_2O_3 glass Series	500	TeO – Te Banding
		650	Stretching Vibration of TeO_4
		750	TeO_4 stretching/B–O–B bending vibrations
		1100	Te–O stretching in TeO_3 units
		1250	BO_3 shoulder
		1380	Vibrations of BO_3
(ii)	Er_2O_3 NPs Series	500	TeO – Te Banding
		650	Stretching Vibration of TeO_4
		750	TeO_4 stretching/B–O–B bending vibrations
		1100	Te–O stretching in TeO_3 units
		1250	BO_3 shoulder
		1380	Vibrations of BO_3



(i) FTIR of Er_2O_3 (ii) FTIR of Er_2O_3 NPs

Fig. 3. FTIR results of the new formulation of zinc boro-tellurite glass system for $\{[(TeO_2)_{0.65}(B_2O_3)_{0.35}]_{0.65}(ZnO)_{0.35}\}_{1-x}$ $(Er_2O_3 / Er_2O_3\ NPs)_x$ glass system.

3.4 Density and molar volume

The density and molar volume data for the zinc boro-tellurite glass system $\{[TeO_2]_{0.65}(B_2O_3)_{0.35}]_{0.65}(ZnO)_{0.35}\}_{1-x}$ $(Er_2O_3 / Er_2O_3\ NPs)_x$ are summarized in Table 2 and illustrated in Figs. 4 and 5. For both the Er_2O_3-doped series and the Er_2O_3-nanoparticle-doped series, density exhibits a clear increasing trend with rising dopant concentration: from 4.441 to 4.949 g cm^{-3} in the Er_2O_3 series and from 5.225 to 5.466 g cm^{-3} in the nanoparticle series. Concurrently, molar volume decreases overall from 30.73 to 28.29 $cm^3\ mol^{-1}$ for Er_2O_3 glasses and from 26.12 to approximately 25.61 $cm^3\ mol^{-1}$ for the nanoparticle series, indicating progressive compaction of the glass network. The substantially higher density and lower molar volume observed for the nanoparticle-doped glasses relative to their ordinary counterparts arise from the more efficient

packing and greater structural compactness conferred by the nanoscale particles, which fill interstitial spaces more effectively than bulk Er_2O_3. These trends are attributed to the substitution of lighter network-forming cations (Te^{4+}, B^{3+}) by the much heavier Er^{3+} ions, which increases the average molecular weight of the glass, together with the generation of non-bridging oxygen that further densifies the structure. Recent studies on Er_2O_3- and Er_2O_3-NP-doped zinc borotellurite and related borotellurite systems have also shown such increases in density and decreases (or ultimate stabilization) in molar volume as the erbium content increases, which indicates that the incorporation of heavy rare-earth ions, especially in the form of nanoparticles, results in increased compactness of the material while maintaining the amorphous nature of the host (Hamza et al., 2020; Al-Buriahi et al., 2025). Such densification is beneficial for photonic applications. Indeed, a higher density is generally associated with better mechanical properties and refractive index. Also, a lower molar volume favors a more rigid network, ideal for optical fiber and laser-host materials.

Table 2. Density and molar volume of Er_2O_3 and Er_2O_3NPs-doped zinc borotellurite glass system

Sample X	Density (g/cm^3)	Molar volume (cm^3/mol)
(a) Ordinary		
0.005	4.441	30.73
0.010	4.554	30.12
0.015	4.621	29.84
0.020	4.736	29.27
0.025	4.888	28.50
0.030	4.949	28.29
(b) Glass with nanoparticles		
0.005	5.225	26.12
0.010	5.279	25.99
0.015	5.399	25.54
0.020	5.426	25.54
0.025	5.443	25.59
0.030	5.466	25.61

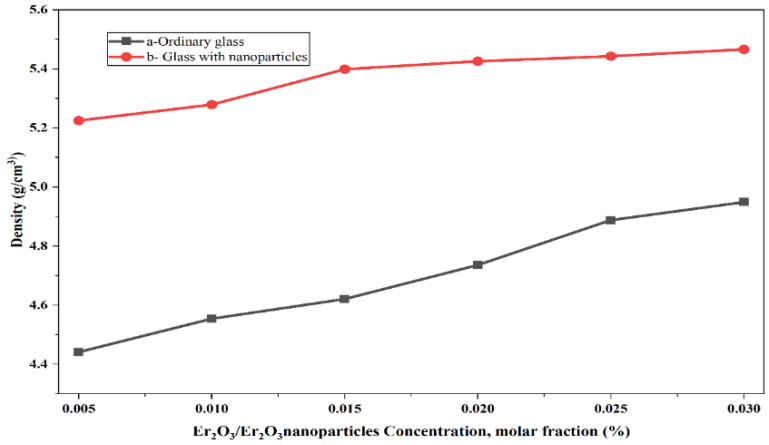


Fig. 4. Density of a-ordinary glass and b-glass with nanoparticles

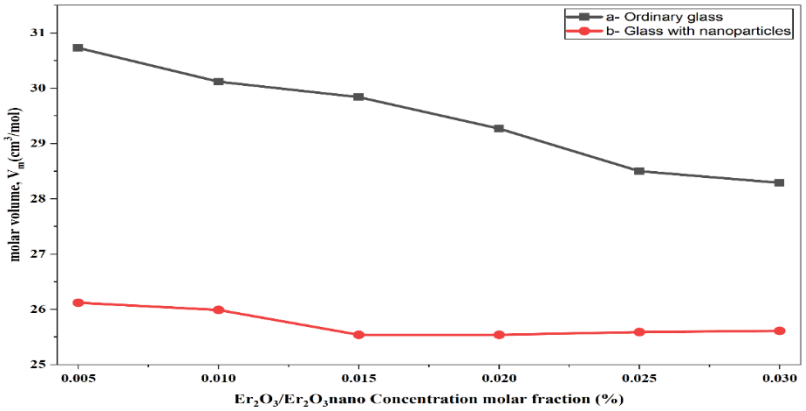
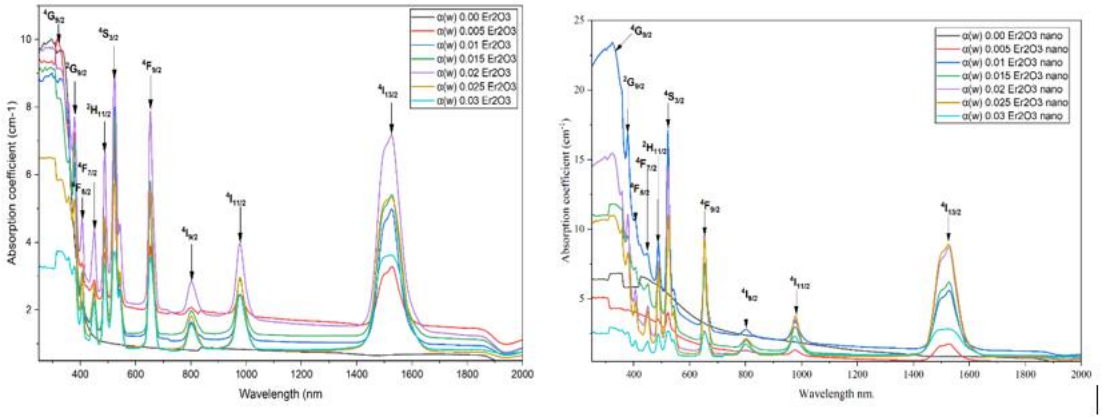


Fig. 5. Molar volume of a-ordinary glass and b-glass with nanoparticles

3.5 Optical Properties



(i) Optical absorption coefficient spectra of Er_2O_3

(ii) Optical absorption coefficient spectra of Er_2O_3 NPs

Fig. 6. Optical absorption coefficient spectra of $\{[(TeO_2)_{0.65}\ (B_2O_3)_{0.35}]_{0.65}\ (ZnO)_{0.35}\}_{1-x}\ (Er_2O_3\ /Er_2O_3\ NPs)_x$ glass system

The optical absorption coefficient spectra of the zinc boro-tellurite glass system $\{[TeO_2]_{0.65}\ (B_2O_3)_{0.35}]_{0.65}\ (ZnO)_{0.35}\}_{1-x}\ (Er_2O_3\ /\ Er_2O_3\ NPs)_x$ are presented in Fig. 6 for both the Er_2O_3-doped series (panel i) and the Er_2O_3-nanoparticle-doped series (panel ii). Both series exhibit a series of sharp, well-resolved absorption bands characteristic of the 4f-4f electronic transitions of Er^{3+} ions from the ground state $^4I_{15/2}$ to various excited levels. The principal bands observed in the visible-to-near-infrared region correspond to transitions to $^4F_{7/2}$ (~488 nm), $^2H_{11/2}$ (~520–522 nm), $^4S_{3/2}$ (~540–545 nm), $^4F_{9/2}$ (~650–655 nm), $^4I_{9/2}$ (~800 nm), $^4I_{11/2}$ (~980 nm), and the technologically important $^4I_{13/2}$ level (~1530–1535 nm).

The intensity of these absorption peaks increases systematically with rising Er_2O_3 (or Er_2O_3 NPs) concentration, confirming the progressive incorporation of optically active Er^{3+} ions into the glass network without significant clustering or precipitation. The overall spectral profiles of the ordinary and nanoparticle series are closely similar, although the nanoparticle-doped glasses generally display slightly lower peak intensities at equivalent molar fractions, consistent with differences in local-field environment and polarizability arising from the

nanoscale particle size. The observed absorption bands are in good agreement with the reported bands for Er^{3+} doped zinc borotellurite, zinc-tellurite and related boro-tellurite glasses in the recent literature, where the same set of 4f–4f transitions are routinely observed and assigned, confirming the successful doping and suitability of the host for photonic applications like optical amplifiers and near-infrared lasers operating around 1.53 μm (Kaur et al., 2020; Lakshminarayana et al., 2023; Umar et al., 2021). The presence of the strong $^4I_{15/2} \rightarrow {}^4I_{13/2}$ absorption band near 1.53 μm is particularly significant, as it underpins the potential of these glasses for C-band fiber-amplifier and laser applications.

5.6 Optical dispersion analysis

The refractive-index dispersion behaviour of the zinc boro-tellurite glass system $\{[TeO_2]_{0.65}(B_2O_3)_{0.35}]_{0.65}(ZnO)_{0.35}\}_{1-x}(Er_2O_3 / Er_2O_3\ NPs)_x$ is presented in Fig. 7. Panel (a) shows the wavelength dependence of the refractive index for selected compositions of both the Er_2O_3 and Er_2O_3-nanoparticle series; all curves exhibit the classic normal dispersion characteristic of dielectric glasses, with refractive index decreasing smoothly from the visible toward the near-infrared. Panel (b) quantifies the refractive index at three technologically relevant fixed wavelengths (589 nm, 632.8 nm and 1550 nm) as a function of dopant concentration, while panel (c) displays the corresponding Sellmeier fits that accurately describe the measured dispersion.

In both series, the refractive index rises with increasing Er_2O_3 (or Er_2O_3 NPs) content, an effect attributable to the higher polarizability of Er^{3+} ions relative to the host cations, the concomitant increase in density, and the progressive formation of non-bridging oxygen that enhances electronic polarizability. The nanoparticle-doped glasses consistently display higher refractive-index values than their ordinary counterparts at equivalent molar fractions, consistent with the denser packing and greater local-field enhancement conferred by the nanoscale particles. These trends are in excellent agreement with recent reports on Er^{3+}- and Er_2O_3-NP-doped zinc borotellurite and related tellurite systems (2020–2025), which likewise document an increase in refractive index with rare-earth concentration and successful description of the dispersion by Sellmeier equations (Umar et al., 2021; El-Mallawany et al., 2021; Laoding et al., 2023).

The elevated refractive indices (typically >1.90 across the visible–NIR window) together with the smooth, low-dispersion behaviour make the present glasses attractive candidates for photonic applications such as optical waveguides, fibre amplifiers and nonlinear optical devices operating in the telecommunications window around 1550 nm.

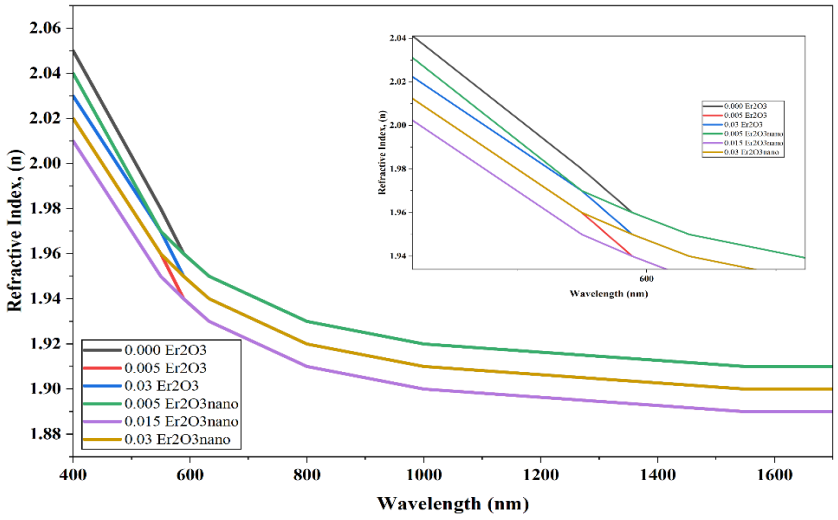


Figure 7 (a) Refractive index as a function of wavelength for selected compositions of the Er_2O_3/Er_2O_3NPs series.

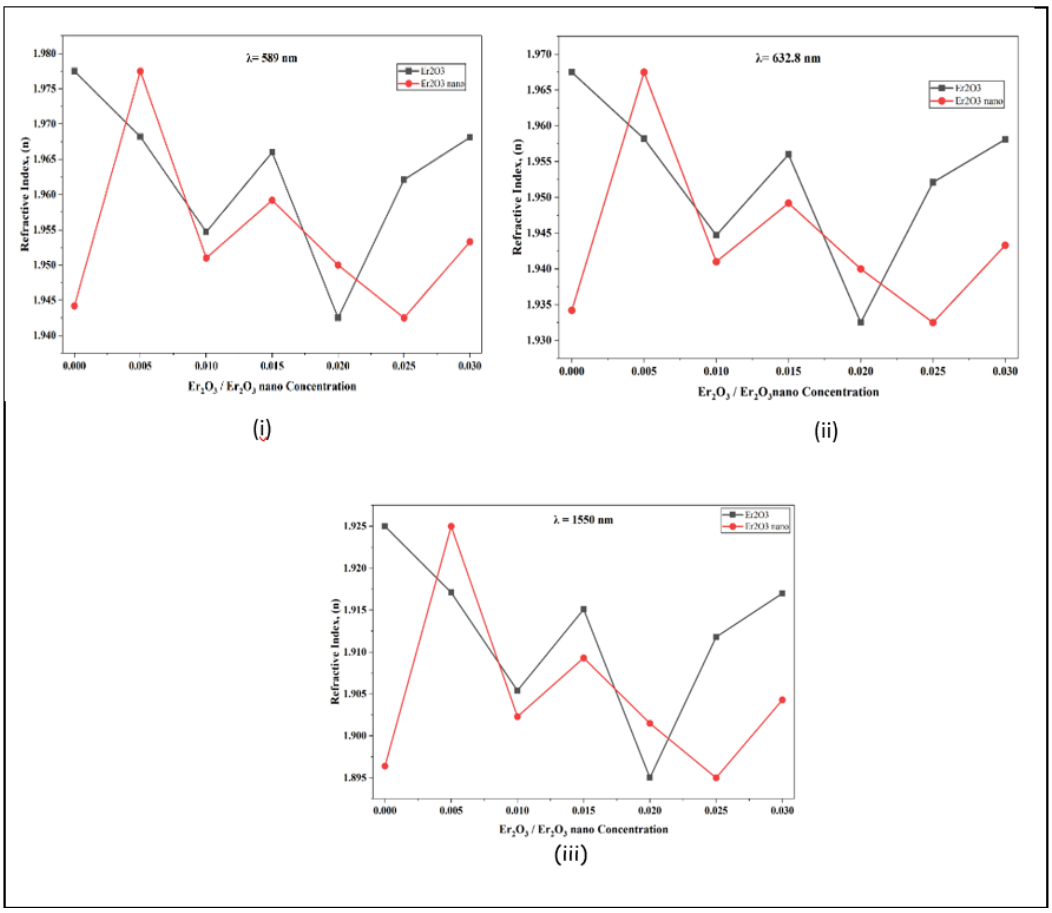


Figure 7 (b) Refractive index at a fixed wavelength (e.g., 589 nm, 632.8 nm and 1550 nm) versus Er_2O_3/Er_2O_3NPs concentration.

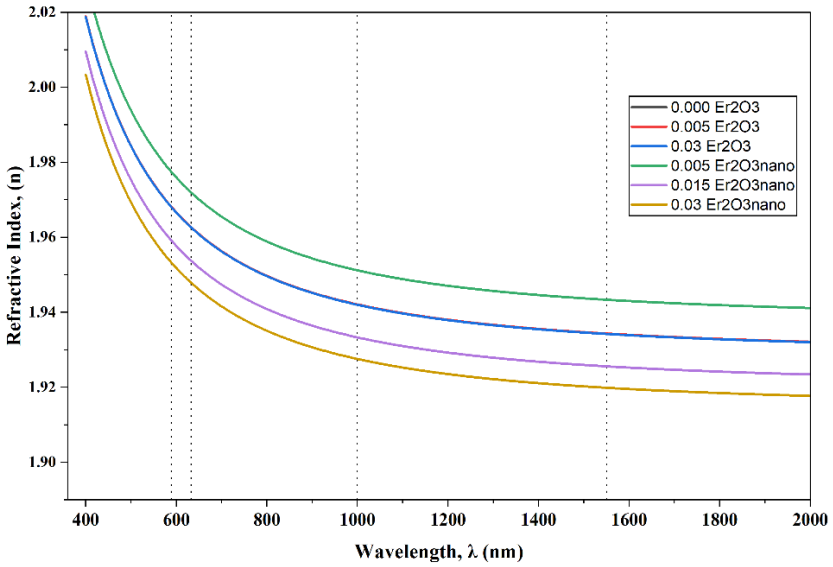


Figure 7 (c)Sellmeier fitting curves for representative samples

Figures 7. (a), (b), and (c) Optical dispersion analysis

3.7 Indirect bandgap and Urbach energy

The indirect optical bandgap (E_g) and Urbach energy (E_U) of the zinc boro-tellurite glass system, $\{[TeO_2]_{0.65}\ (B_2O_3)_{0.35}]_{0.65}\ (ZnO)_{0.35}\}_{1-x}$ (Er_2O_3 / Er_2O_3 NPs)$_x$ are presented in **Figs. 8 and Fig. 9** and summarised in **Table 3**. Both glass series exhibit a systematic decrease in E_g with increasing Er_2O_3 concentration, from 2.954 to 2.568 eV for the conventional Er_2O_3-doped glasses and from 3.061 to 2.390 eV for the Er_2O_3 nanoparticle-doped glasses. In parallel, E_U increases from 0.315 to 0.675 eV and from 0.340 to 0.800 eV for the conventional and nanoparticle-doped series, respectively. The gradual decrease of E_g indicates a shift of the absorption edge to lower photon energies, while the increase of E_U reveals broadening of the exponential absorption tail and an increase of the structural/electronic disorder

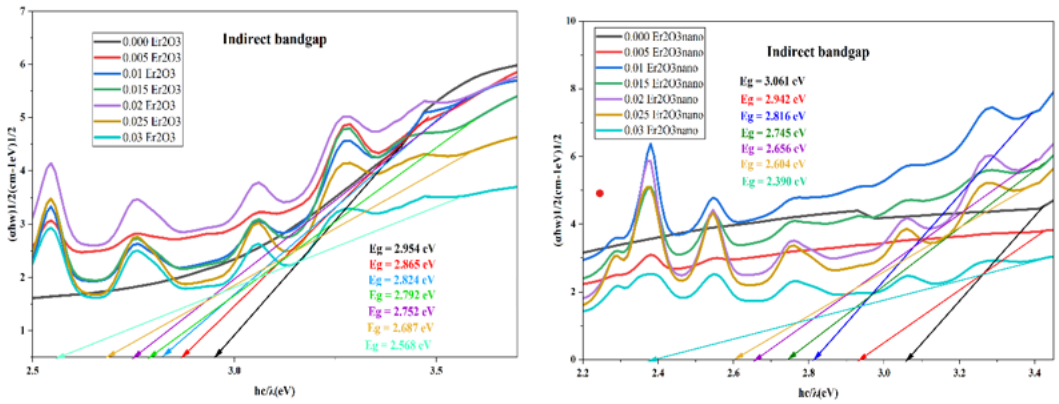
The decrease in E_g is attributed to Er^{3+}-induced modifications of the glass network, such as changes in the relative populations of bridging and non-bridging oxygen environments, local bonding configurations and defect-related or localized electronic states. Such structural changes can introduce additional states near the band edges that can reduce the effective optical bandgap. The concomitant increase in E_U supports this interpretation as the broadening of the absorption tail is indicative of increasing fluctuations in the local structural and electronic environment with increasing dopant concentration. Thus, the inverse correlation between E_g and E_U indicates that progressive Er_2O_3 incorporation simultaneously modifies the electronic absorption edge and increases the degree of disorder within the glass network.

At comparable molar fractions, the Er_2O_3 nanoparticle-doped glasses generally exhibit a larger reduction in E_g and higher E_U values than the conventional Er_2O_3-doped glasses. This difference suggests that nanoparticle incorporation produces a stronger modification of the local glass environment, potentially through interfacial effects, altered dopant distribution, and enhanced local structural perturbation associated with the nanoscale Er_2O_3 phase. However, these mechanisms should be regarded as plausible interpretations rather than direct evidence of enhanced NBO generation, unless independently supported by complementary structural characterisation.

The decrease of Eg with increase of EU is consistent with the behavior usually reported for rare-earth doped tellurite and borotellurite glasses (Umar et al., 2021; Laoding et al., 2023). All these results indicate that the addition of Er_2O_3, especially in the form of nanoparticles, is a good way to tailor the absorption edge and the optical disorder level of zinc boro-tellurite glasses. Such compositional control is relevant to the design of rare-earth-doped glasses with tailored optical dispersion and absorption characteristics for photonic and fibre-optic applications.

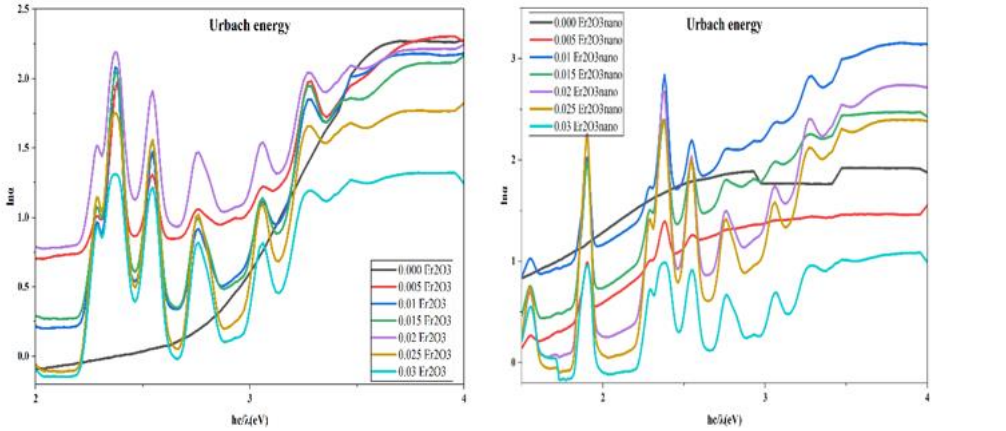
Table 3. Calculated value parameters of Er_2O_3 and Er_2O_3NPs doped zinc borotellurite glasses.

Sample ID	0.000	0.005	0.010	0.015	0.020	0.025	0.030
(a) Ordinary							
Indirect bandgap (eV)	2.954	2.865	2.824	2.792	2.752	2.687	2.568
Urbach Energy (eV)	0.315	0.360	0.430	0.500	0.560	0.615	0.675
(b) Glass with nanoparticles							
Indirect bandgap (eV)	3.061	2.942	2.816	2.745	2.656	2.604	2.390
Urbach Energy (eV)	0.340	0.400	0.485	0.575	0.650	0.725	0.800



(i) Indirect bandgap Er_2O_3 (ii) Indirect bandgap Er_2O_3 NPs

Fig. 8. Indirect bandgap of $\{[(TeO_2)_{0.65}(B_2O_3)_{0.35}]_{0.65}(ZnO)_{0.35}\}_{1-x}(Er_2O_3/Er_2O_3\ NPs)_x$ glass system



(i) Urbach energy Er_2O_3 (ii) Urbach energy Er_2O_3 NPs

Fig. 9. Urbach energy of $\{[(TeO_2)_{0.65}(B_2O_3)_{0.35}]_{0.65}(ZnO)_{0.35}\}_{1-x}(Er_2O_3/Er_2O_3NPs)_x$ glass system.

4. Conclusion

Zinc borotellurite glasses containing conventional Er_2O_3 and Er_2O_3 nanoparticles were successfully synthesised and systematically investigated in terms of their structural and optical properties. Both dopant forms preserved the amorphous character of the host glass while producing concentration-dependent modifications of the local glass network, as indicated by FTIR, density and molar-volume measurements. Er_2O_3 incorporation increased the density and reduced the molar volume, with the nanoparticle-doped glasses exhibiting consistently higher densities and lower molar volumes than the conventional Er_2O_3 series at comparable molar fractions, indicating greater structural compaction. The optical response was also strongly dependent on both dopant concentration and physical form. The refractive index increased with Er_2O_3 incorporation, while the indirect optical band gap decreased from 2.954 to 2.568 eV for the conventional series and from 3.061 to 2.390 eV for the nanoparticle series. Concurrently, the Urbach energy increased from 0.315 to 0.675 eV and from 0.340 to 0.800 eV, respectively, indicating progressive broadening of the absorption tail and increased structural/electronic disorder. These changes are consistent with dopant-induced modifications of the local bonding environment, including changes in bridging and non-bridging oxygen configurations,

together with the contribution of the highly polarizable Er^{3+} ions to the optical response. The more pronounced changes observed for the nanoparticle-doped glasses suggest that the physical form of the erbium precursor provides an additional means of modifying the local structure and optical properties of the host network. Overall, the results demonstrate that both Er_2O_3 concentration and dopant form can be used to tailor refractive-index dispersion, optical band-gap characteristics and absorption-edge disorder in zinc borotellurite glasses. The combination of enhanced refractive index, tunable absorption edge and the technologically relevant Er^{3+} transition around 1.53 μm highlights the potential of these materials for near-infrared photonic and fibre-optic applications, including Er^{3+}-based optical amplification and integrated optical components.

References

Azlan, M. N., Halimah, M. K., & Sidek, H. A. A. (2017). Linear and nonlinear optical properties of erbium doped zinc borotellurite glass system. *Journal of Luminescence, 181*, 400–406. https://doi.org/10.1016/j.jlumin.2016.09.045

Azlan, M. N., Halimah, M. K., Sidek, H. A. A., & Daud, S. (2013). Effect of erbium nanoparticles on optical properties of zinc borotellurite glass system. *Journal of Nanomaterials*, 2013, Article 940917. https://doi.org/10.1155/2013/940917

Azlan, M. N., Halimah, M. K., Suriani, A. B., Azlina, Y., & Umar, S. A. (2024). Borotellurite bio-silica glasses doped by erbium nanoparticles: Structural and thermal properties. *Journal of Theoretical and Applied Physics*. https://doi.org/10.30495/jtap.162220

Azlan, M. N., Halimah, M. K., Suriani, A. B., Azlina, Y., & Umar, S. A. (2016). Optical properties of zinc borotellurite glass system doped with erbium and erbium nanoparticles for photonic applications. *Journal of Materials Science: Materials in Electronics*, 28, 4318–4327. https://doi.org/10.1007/s10854-016-6056-2

El-Mallawany, R., Ribeiro, M. A., Lara, L. S., Lenzi, E. K., Alsadig, I. A. A., & Novatski, A. (2021). Refractive index behavior of tellurite glasses. *Optical Materials*, 112, 110810. https://doi.org/10.1016/j.optmat.2020.110810

Gowda, G. V. J., Deka, U., Dahshan, A., Reddy, G. V. A., Eraiah, B., Gedam, R. S., Keshavamurthy, K., & Devaraja, C. (2024). Exploration of physical, structural, thermal, and optical properties of alkali zinc boro tellurite glasses doped with europium trioxide. *Applied Physics A, 130*, 777. https://doi.org/10.1007/s00339-024-07920-x

Hamza, A. M., Aliyu, U. S., Kamari, H. M., Geidam, I. G., El-Mallawany, R., Nazrin, N., & Baba, M. N. (2022). Borotellurite bio-silica glasses doped by erbium nanoparticles: Structural and thermal properties. *Journal of Theoretical and Applied Physics, 16*(2), 1–7. https://doi.org/10.30495/jtap.162220

Hamza, A. M., Halimah, M. K., Muhammad, F. D., & Chan, K. T. (2020). Structural, elastic and thermo-physical properties of erbium oxide nanoparticles doped bio-silicate borotellurite glass system. *SN Applied Sciences*, 2, 291. https://doi.org/10.1007/s42452-020-2112-x

Kaur, S., Pandey, O. P., Jayasankar, C. K., & Chopra, N. (2020). Influence of heat treatment on spectroscopic and structural properties of vitreous Er3+-doped zinc borotellurite. *Journal of Non-Crystalline Solids*, *530*, 119842.

Kraskowski, I., Nasser, K., Korri, J., Närhi, M., Gumenyuk, R., Othmani, A., ... & Petit, L. (2025). Unveiling the advances and challenges in the development of Er3+-doped tellurite fiber with embedded Ag nanoparticles. *Journal of the American Ceramic Society*, *108*(5), e20385.

Lakshminarayana, G., Meza-Rocha, A. N., Soriano-Romero, O., Caldiño, U., Lira, A., & Yoon, J. (2023). Er^{3+}: B_2O_3-TeO_2-ZnO-PbF_2–M_2O/MF (M = Li, Na, and K) glasses: An inspection of structural, thermal, optical, chromatic, and near-infrared luminescence traits for displays

and potential C-band amplification. *Journal of Non-Crystalline Solids*, 622, 122660. https://doi.org/10.1016/j.jnoncrysol.2023.122660

Laoding, H., Mohamed Kamari, H., Amat, A., & Saroni, A. (2023). Optical properties of cerium oxide doped zinc borotellurite glass. *Scientific Research Journal*, 20(1), 13–32. https://doi.org/10.24191/srj.v20i1.19091

Lemiere, A., Bondzior, B., Aromäki, I., & Petit, L. (2022). Study of visible, NIR, and MIR spectroscopic properties of Er3+-doped tellurite glasses and glass-ceramics. *Journal of the American Ceramic Society*, *105*(12), 7186-7195.

Rafien, S. N. M., Kasim, A., Hashim, A., Razali, W. A. W., & Yahya, N. (2020). Fourier Transform Infrared Spectroscopy and Optical Properties of Samarium Doped Zinc Borotellurite Glasses. *Malaysian Journal of Analytical Sciences*, *24*(5), 736-743.

Ngaram, S. M., Hashim, S., Sanusi, M. S. M., Ibrahim, A., & Sayyed, M. I. (2025). Structural and optical characteristics of B_2O_3-TeO_2-Bi_2O_3-$SrCO_3$-K_2CO_3-Er_2O_3 glass systems: Role of Er^{3+} doping. *Ceramics International, 51*(5), 5882–5889. https://doi.org/10.1016/j.ceramint.2024.12.xxx

Preethi, H., Devaraja, C., & Deka, U. (2026). A review on transition metal oxide nanoparticles and rare earth oxide doped borate and tellurite glasses: From structural, optical, and photoluminescence properties to next generation optical technology. *Journal of Alloys and Compounds, 1062*, 187590. https://doi.org/10.1016/j.jallcom.2026.187590

Al-Buriahi, M. S., Alomayrah, N., Owoeye, S. S., & Alsaiari, N. S. (2025). Effects of Er2O3 doping on the physical properties and gamma/neutron shielding performance of borate-tellurite glasses: PHITS Monte Carlo simulations. *Radiation Physics and Chemistry*, *237*, 113042.

Singh, V., Rautela, M. S., & Singh, N. (2024). Investigating the effect of gamma irradiation on structural and optical properties of (55-x)TeO_2–20ZnO–25B_2O_3–xEr_2O_3 radiation shielding glass: Influence of Er^{3+} ions. *Radiation Physics and Chemistry*. https://doi.org/10.1016/j.radphyschem.2024.112071

Umar, S. A., Halimah, M. K., Chan, K. T., & Latif, A. A. (2020). Structural, elastic and thermo-physical properties of Er_2O_3 nanoparticles doped bio-silicate borotellurite glasses. *SN Applied Sciences, 2*, 2112. https://doi.org/10.1007/s42452-020-2112-x

Umar, S. A., Halimah, M. K., et al. (2021). Spectroscopic investigations of Er_2O_3 doped silica borotellurite glasses. *Optical Materials*, 114, 110987. https://doi.org/10.1016/j.optmat.2021.110987

Umar, S. A., Halimah, M. K., Geidam, I. G., Alade, I. O., Noorazlan, A. M., Hamza, A. M., & Ahmad, A. F. (2021). Spectroscopic investigations of Er_2O_3 doped silica borotellurite glasses. *Optical Materials*, 114, 110987. https://doi.org/10.1016/j.optmat.2021.110987